J Nanostruct 16(2): 1848-1861, Spring 2026

RESEARCH PAPER

Er-Doped SnO_2 as an Electron Transport Layer for Efficient Inorganic $MAPbI_3$ Perovskite Solar Cells with Improved Performance

Pirooz Shirazi [1], *Mahdiyeh Esmaeili-Zare* [1] *, *Mohsen Behpour* [1,2] *

[1] *Institute of Nanoscience and Nanotechnology, University of Kashan, 87317-51167 Kashan, Iran*

[2] *Department of Analytical Chemistry, Faculty of Chemistry, University of Kashan, 87317-51167 Kashan, Iran*

ARTICLE INFO

Article History:
Received 18 December 2025
Accepted 21 March 2026
Published 01 April 2026

Keywords:
$CH_3NH_3PbI_3$
Electron transport layer
Er-doped SnO_2
Perovskite solar cell
SnO_2

ABSTRACT

Perovskite solar cells (PSCs) have garnered great attention from researchers, and their excellent photovoltaic properties are rapidly advancing. The compact layer is a crucial component of PSCs, facilitating the transport of holes and electrons. Erbium doping, which has a radius comparable to that of tin, enhances the performance of the compact layer by increasing conductivity and improving the device's photoelectric efficiency through the creation of oxygen vacancies and tin (IV) ions. Variable doping concentrations of Er-SnO_2 compact layers were prepared for use in planar-architecture perovskite solar cells (PSCs). Doping of 7.00% erbium in the SnO_2 compact layer indicated that the ITO/Er:SnO_2/$MAPbI_3$/CuPc/Au cell achieves a current density of approximately 12.68 $mA.cm^{-2}$ compared to the ITO/SnO_2/$MAPbI_3$/CuPc/Au cell, which has a current density of about 2.40 mA/cm^2. This important enhancement refers to the light absorption characteristics of Er:SnO_2/ $MAPbI_3$ and the rapid electron and hole transfer processes in Er:SnO_2 and CuPc. In this research, we studied the power conversion efficiency (PCE) of solar cells. The results showed that a significant enhancement in photovoltaic properties can be achieved by utilizing spin-coated CuPc nanoparticles as the hole transport layer, with an increase of at least 5% compared to the ITO/SnO_2/$MAPbI_3$/CuPc/Au Structure.

How to cite this article
Shirazi P., Esmaeili-Zare M., Behpour M. Er-Doped SnO_2 as an Electron Transport Layer for Efficient Inorganic $MAPbI_3$ Perovskite Solar Cells with Improved Performance. J Nanostruct, 2026; 16(2):1848-1861. DOI: 10.22052/JNS.2026.02.035

INTRODUCTION

Due to their low cost, robust light absorption capacity, solution-based preparation method, adjustable band gap, and extended carrier diffusion length, organic-inorganic lead hybrid perovskites are becoming increasingly popular among researchers worldwide. It is also an ideal material for light-absorbing material in solar cells [1-3]. Within just a few years of the introduction of perovskite solar cells in 2009, the power conversion efficiency of solar cells utilizing perovskite materials for light absorption has surged from 3.8% to 25.5% [4-10]. The most common components of PSCs are an electron transport layer (ETL), a hole transport layer (HTL), and a counter electrode and also, there are bipolar electron

* *Corresponding Author Email: m.behpour@kashanu.ac.ir*

and hole transport properties in perovskites [11-13]. In the course of PSCs development, devices without HTL and an electron-free transport layer structure have emerged to reduce the cost of the device and simplify the preparation process [14, 15]. By utilizing this arrangement, the present device has showed the PCE about 15.7% [5, 16-19]. The performance of the device is determined by the compact layer, which blocks holes and transports electrons. Light transmission, minimal surface imperfections, uniform and dense film formation, hole-blocking ability, electron mobility, and an energy band structure compatible with perovskite materials are some of the criteria for a brilliant compact layer. SnO_2 as a semiconductor of the n-type, is an ideal compact layer material because of its good UV stability, relatively low conduction band bottom, and high electron mobility (~240 $cm^2 V^{-1} s^{-1}$) [20-22]. The SnO_2 layer is prepared using numerous methods, including chemical bath deposition, atomic layer deposition, and spray pyrolysis [23-28]. For PSCs to achieve superior band alignment and charge transport, the compact layer's surface contact and electrical properties must be enhanced. Commonly employed optimization techniques encompass surface treatment, metal cation doping, and the development of composite materials. Rao et al. achieved a remarkable boost in the power conversion efficiency (PCE) of the device, increasing it from 6.5% to 14.6%, by applying an aqueous $TiCl_4$ solution to treat the SnO_2 compact layer's surface [29]. To enhance the electrical conductivity of the SnO_2 compact layer and decrease the conduction band energy of SnO_2, Park et al. used Li-doped SnO_2. The result was the facilitation of the electron transfer from the perovskite layer to the compact layer, thereby achieving the PCE of 18.2% [30]. Bai et al. augmented the electrical conductivity of the SnO_2 compact layer by doping it with Sb, thereby enhancing its Fermi energy level. This resulted in a greater transfer of charges while effectively preventing the recombination of carriers, leading to the PCE elevating from 15.7% to 17.2% [31]. Liu et al. combined the advantages of TiO_2 and Mg-doped SnO_2 to produce a composite compact layer with outstanding capabilities. Therefore, they observed an increase in the PCE of the device from 11.85% to 13.01% [32]. Liu et al. combined the advantages of TiO_2 and Mg-doped SnO_2 to produce a composite compact layer with outstanding capabilities. Therefore, they observed an increase in the PCE of the device from 11.85% to 13.01% [33]. Doping metal ions in the electron transfer layers improves the optoelectronic properties of perovskite solar cells by increasing the energy level between them and the perovskite material, thus modifying its energy band [34-38].

In this study, we initially used the compact layer of erbium doped with SnO_2 for planar PSCs, with the PCE achievement of 6.07%. During the annealing process, erbium doping affects the crystallization of SnO_2, resulting in perfect film coverage without crystal aggregation and pin-holes. Furthermore, erbium doping improves the conductivity of the SnO_2 layer and results in an upward shift of the conductive band minimum (CBM), which contributes to the increase in V_{oc} and suppresses the hysteresis behavior. As demonstrated by the simple interfacial control approach presented in this study, Er doping is a feasible strategy for improving the performance of perovskite solar cells.

MATERIALS AND METHODS

Material

The purchased materials are as follows: anhydrous tin(IV) chloride ($SnCl_4$, 99.95%), ($Er(NO_3)_3$, 99.8%), anhydrous ethanol, anhydrous dimethylsulfoxide (DMSO, 99.9%), anhydrous dimethylformamide (DMF, 99.8%), Chloro benzen, and Ethanol from Wako, Japan; Lead nitrate, Potassium iodide, ITO (10 Ω/sq) was bought from Sepahan Gostar. phthalic anhydride, urea, copper chloride dihydrate, ammonium molybdate, boric acid was purchased from Merck company. No further purification is performed on the solvents before utilizing them.

Constructing ETL

ITO substrates were washed by sonication with detergents, DI water, acetone and isopropanol consecutively for 15 min. First, to make SnO_2 ETLs, pure-ethanol and $SnCl_4$ were selected as precursors. The ITO/SnO_2 structure was prepared by dissolving $SeCl_4$ in ethanol solvent with a concentration of 0.07M. Next, the Er doped SnO_2 structures were synthesized by adding appropriate amount of $Er(NO_3)_3$ in the precursor solution. All layers were coated using the spin coating method in ambient conditions for 30 s at 3000 rpm. Finally, all the films were sintered at 70°C for 30 min. Thereafter, the SnO_2 or Er:SnO_2 films were subjected to a UV-Ozone (with 200 W power of

UV-C band) treatment with a duration of up to 15 min. It has been reported that the treatment of electron transfer layers with UV-Ozone can increase the wetting of the substrate before coating [37, 38].

Constructing perovskite layer

The Golden Rain method was used to synthesize PbI_2 [36]. To accomplish this, two separate solution containing 0.1 M lead nitrate solution in one beaker and 2 M potassium iodide solution in another beaker were prepared using the distilled water solvent, and then placed on the heater-stirrer at a temperature of 80°C for 2 h. The two solutions are mixed after reaching the desired temperature, triggering the formation of PbI_2 as Golden Rain. Subsequently, methyl ammonium iodide is synthesized as follows: A mixture of 30 ml methylamine and 30 ml HI is stirred using magnetic stirrer in the ice bath for 2 h. The result solution is rested for 24 h. Afterwards; it is heated to 70°C to enable the solvents to evaporate, resulting in the formation of a brown solid matter. Solving this solid in ethanol yields a solution that can recreate the final product. Adding the solution to diethyl ether and crystallizing MAI white crystallites is the next phase. The crystals are separated from the solution by a filter and then dried at room temperature after being washed with diethyl ether.

For precursor perovskite solution of $MAPbI_3$, 0.22 g methylammonium iodide (CH_3NH_3I) and 0.64 g lead iodide (PbI_2) were dissolved in 800 µL DMF and 200 µL DMSO mixture (volume ratio of 4 to 1) and then stirred at 70 °C for 2 h. Then, the samples were deposited by one-step spin coating at 4000 rpm for 34 s. At the last 20 s, 150 µl chlorobenzene solution as antisolvent was added to the substrates and subsequently the samples were subjected to annealing for 10 min at 100°C.

Constructing hole transporting layer

The general procedure employed for syntheses of copper phthalocyanines was described as; phthalic anhydride (0.27 M), urea (1.35 M), and copper chloride dihydrate (0.05 M) with ammonium molybdate as a catalyst were charged together into a 3-neck reaction flask. The reaction flask was placed in a microwave synthetic unit and heated to temperature of 180°C for 45 min. Reaction product was washed with 1N HCl (acid-treated) and 1N NaOH (alkali-treated) solutions for one hour. After filtration, it was dried at 105°C over 2 h in a dry oven, whereupon final product was obtained. The produced CuPc as HTL was settled via spin-coating at a speed of 3000 rpm for

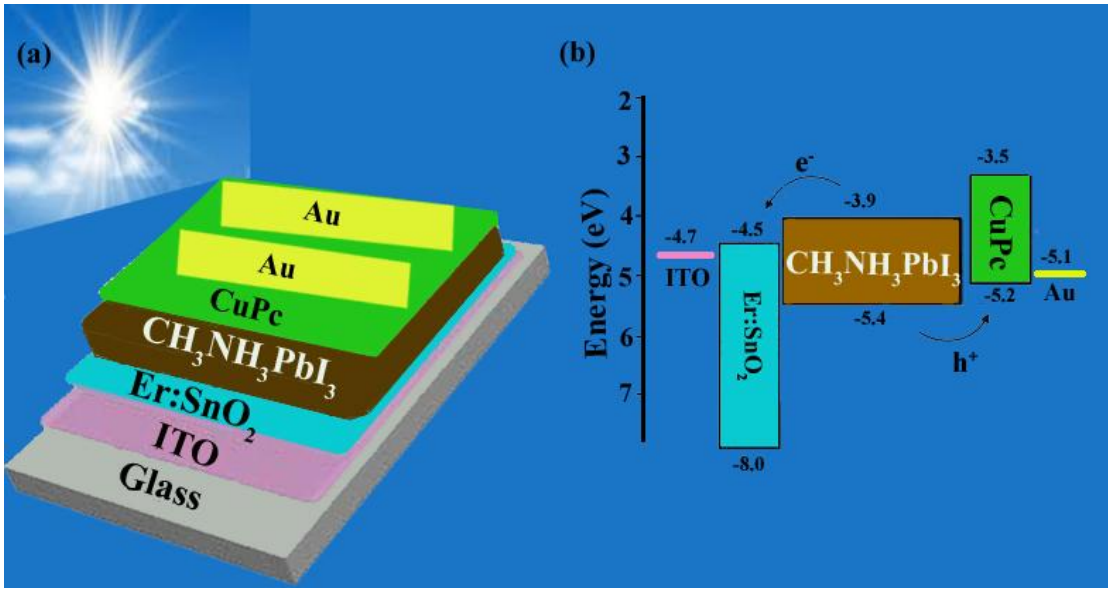

Fig. 1. (a) Schematic device structure of the PSC based on Er:SnO_2 ETL and (b) Energy band diagram of corresponding materials used in the device.

one minute on ITO/ETLs/Perovskite substrate. The produced CuPc as hole transfer layer was settled via spin-coating at a speed of 3000 rpm for one minute on ITO/ETLs/Perovskite substrate. Lastly, a gold cathode with a thickness of 80 nm was edeposited onITO/ETLs/Perovskite/CuPc cell

In this study, a regular cell structure using Er doped SnO_2 as ETL was fabricated, as shown in Fig. 1a. Cathode and anode electrodes were ITO and Au, respectively. Also, electron and hole transfer layers (ETL and HTL) were Er: SnO_2 and CuPc. In order to enhance the performance of the HTL, Er was doped with SnO_2. Fig.1b indicates energy level of PSC's each layer employed in this study. The carrier extraction and transport can be also enhanced using proper interfacial energy level alignment.

RESULTS AND DISCUSSION

Characterization

Characterization of nanoparticle, thin-film, and device: the FE-SEM method employs TESKAN equipped with an EDS morphology system. Structural features of the crystal are investigated using x-ray diffraction (X'Pert Pro MPD, PANalytical). Furthermore, analyzing the transmission and absorption spectrum through UV spectroscopy determines the optical characteristics of sediment layers. A 3-electrode configuration is used to perform cyclic voltammetry of films with different percentages of impurity. Also, a quartz cell and 0.5 molar KCl solution are used to solve the electrolyte solution for Mott-Schottky analysis in a 3-electrode configuration.

The electrodes used for working, reference,

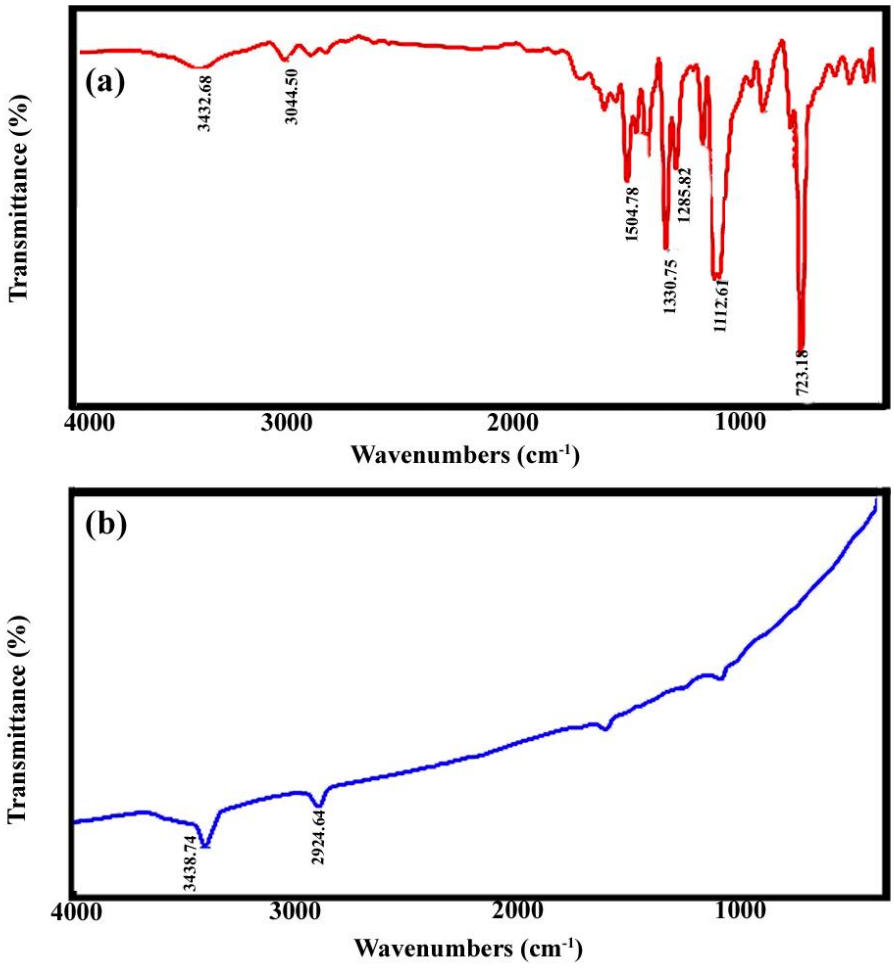

Fig. 2. FT-IR spectra of a) PbI_2 and b) CuPc.

and counter are ITO/Er: SnO_2, Ag/AgCl, and Pt, respectively. With a speed of 50 mV, the bias voltage is measured from -0.6 to 0.4 V. The solar cell was lightened at medium temperature utilizing air conditioners (humidity, approximately 20%) and a solar simulator (AM1.5G, 100 mW cm^{-2}, IVIUMSTAT).

Characterization of nanoparticle (PbI_2, CuPc and MAI)

The PbI_2 nanoparticle and CuPc were characterized by FTIR transmittance spectra, as shown in Fig. 2. Fig. 2a presents the FT-IR spectrum of PbI_2 nanoparticles without any organic components**.** Peaks at 3400 and 1650 cm^{-1} in the FT-IR spectrum are assigned to O-H stretching modes of adsorbed water molecules. However, the broad and strong hydroxyl stretching and bending bands observed around 3400 and 1650 cm^{-1} in the FT-IR spectrum suggest a different type of interaction. These bands are typically associated with adsorbed water molecules, indicating their

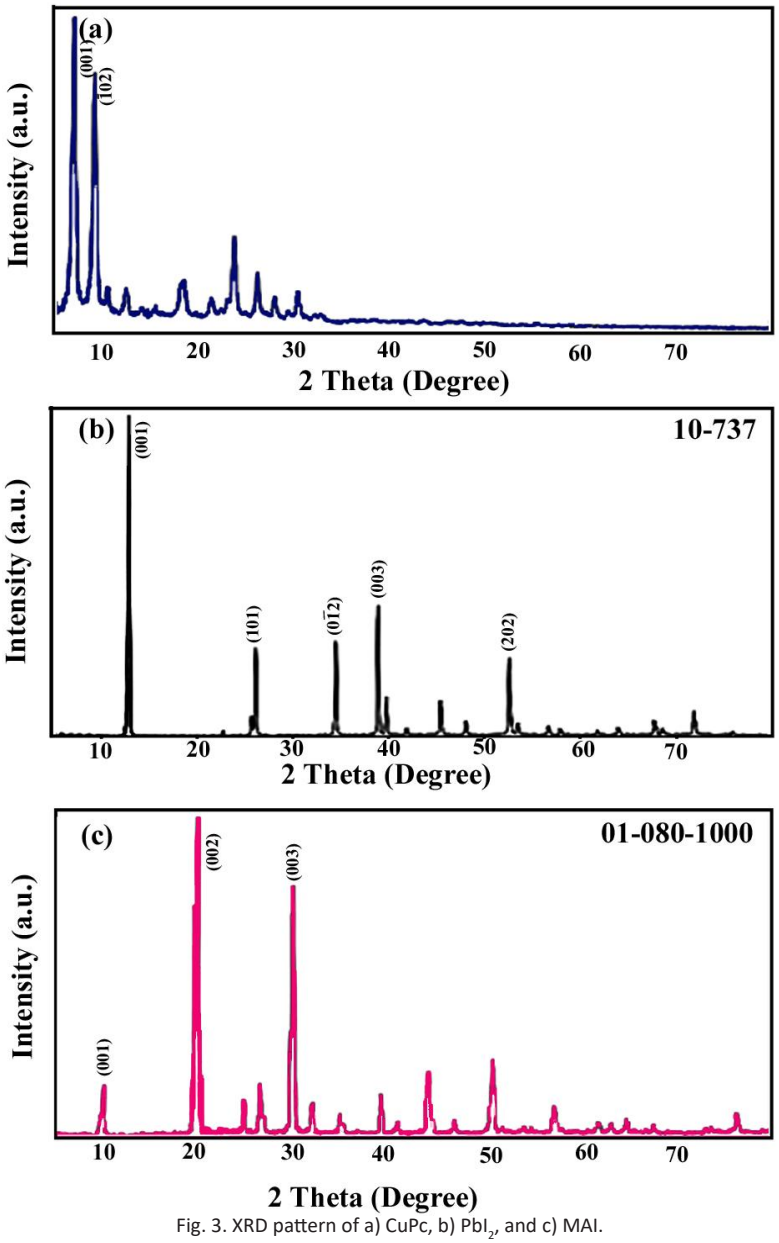

Fig. 3. XRD pattern of a) CuPc, b) PbI_2, and c) MAI.

presence on the PbI_2 nanoparticle surface. While free O-H groups typically exhibit asymmetric and symmetric stretching vibrations around 3756 and 3652 cm^{-1}, respectively, the FT-IR spectrum reveals broader and stronger bands at 3412 and 3383 cm^{-1}. These deviations suggest the presence of hydrogen bonding between the O-H groups and the PbI_2 nanoparticles.

Fig. 2b presents the FT-IR spectrum of CuPc, exhibiting characteristic peaks for aromatic C-H (3044 cm^{-1}), C=C macrocycle (1607 cm^{-1}), C=N (1504 cm^{-1}), C-C in isoindole (1330 cm^{-1}), in-plane C-H bending (1112 cm^{-1}), and out-of-plane C-H bending (723 cm^{-1}). Additional peaks at 1285 cm^{-1} and 1164 cm^{-1} correspond to C-N stretching and in-plane bending in isoindole, respectively.

Fig. 3 represents the XRD spectrum results for synthesized powders. The XRD pattern of CuPc crystals in Fig. 3a exhibits two distinct peaks at 7.07° and 9·24°, corresponding to (001) and ($1^{-}02$) reflections, respectively. These characteristic peaks are attributed to the β-CuPc phase, consistent with observations in previous studies.

The crystal structure of PbI_2 solid nanoparticles was determined using X-ray diffraction (XRD). The results are presented in Fig. 3b. The vital diffraction peaks are placed as (001) at 12.80°, (101) at 25.60°, (003) at 38.70° and (202) at 52.50°. Fig. 3c presents the XRD pattern of methylammonium iodide (MAI), indicating the crystallographic planes associated with the observed peaks. The crystallite sizes of the samples CuPc, PbI_2 and MAI were calculated by Scherrer equation and estimated about 31.51, 57, and 20 nm, respectively.

Figs. 4a and b indicate TEM images that were used to consider and find out the microscopic structure of MAI and CuPc samples at the nanoscale. Fig. 4a clearly indicates that the MAI nanoparticles formed an interjoining nanoparticulate structure. These nanoparticles have a regular shape with diameters ranging from 30 nm to about 100 nm. Such a structure produces a fast electron transport and a low grain boundary. The CuPc TEM image shows homogenous particles, matching with the SEM image (particle size = 50-100 nm). The large, circular nanocrystals in Fig. 4b indicate that these films have a polycrystalline character on a nanoscale.

ETL and device structure

The XRD pattern for the perovskite film formed on the SnO_2 ETLs and CuPc film are shown in Fig. 5(a-c). Fig. 5b presents seven intense and sharp peak positions, corresponding to (110), (112), (220), (310), (224), and (314) crystal planes of perovskite, respectively [11]. The highest intensity of the (110) crystal plane of perovskite is observed when the concentration of SnO_2 colloidal dispersion solution was 5 wt.%. This is due to the presence of a certain roughness on the surface of SnO_2, which facilitates stress release during the annealing of the perovskite layer, resulting in a superior quality of perovskite crystallization with virtually no holes. The XRD pattern of the ITO/Er:SnO_2/$MAPbI_3$/CuPc solar cell (Fig. 5a) shows one diffraction peak at 7.04 degree, that is related to β-CuPc.

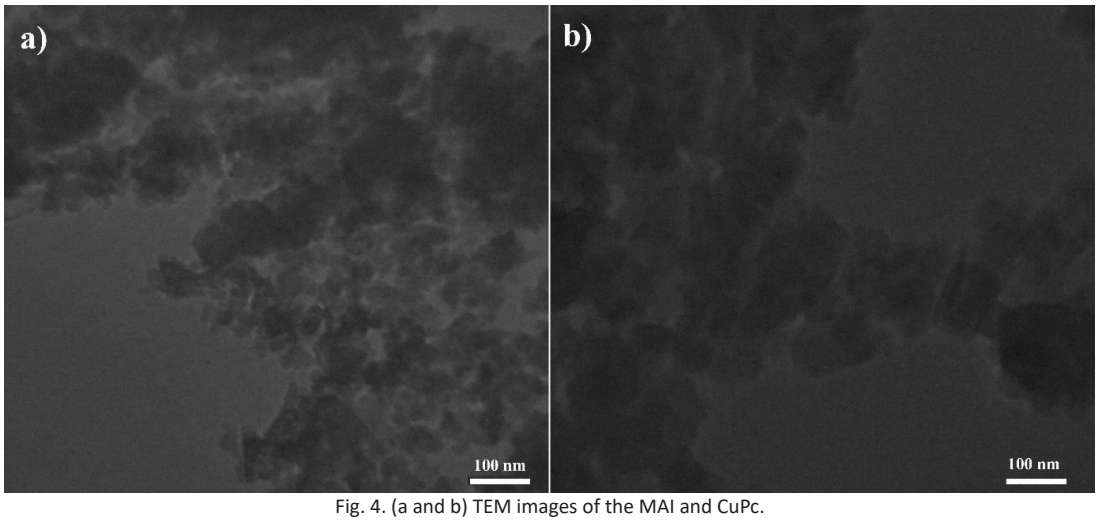

Fig. 4. (a and b) TEM images of the MAI and CuPc.

The top view morphological images of SnO_2 and Er: SnO_2 are shown in Fig. 6. It is believed that the placement of erbium in the SnO_2 lattice reduces the vacancies on the electron transport layer by reducing the surface pin-holes (Fig. 6a, b). A hypothesis has been made that the pin-holes and aggregated island surface may cause strong recombination at the interface between the ETLs and the perovskite layer, which is unfavorable for PSC applications. Lanthanide doping enhances in

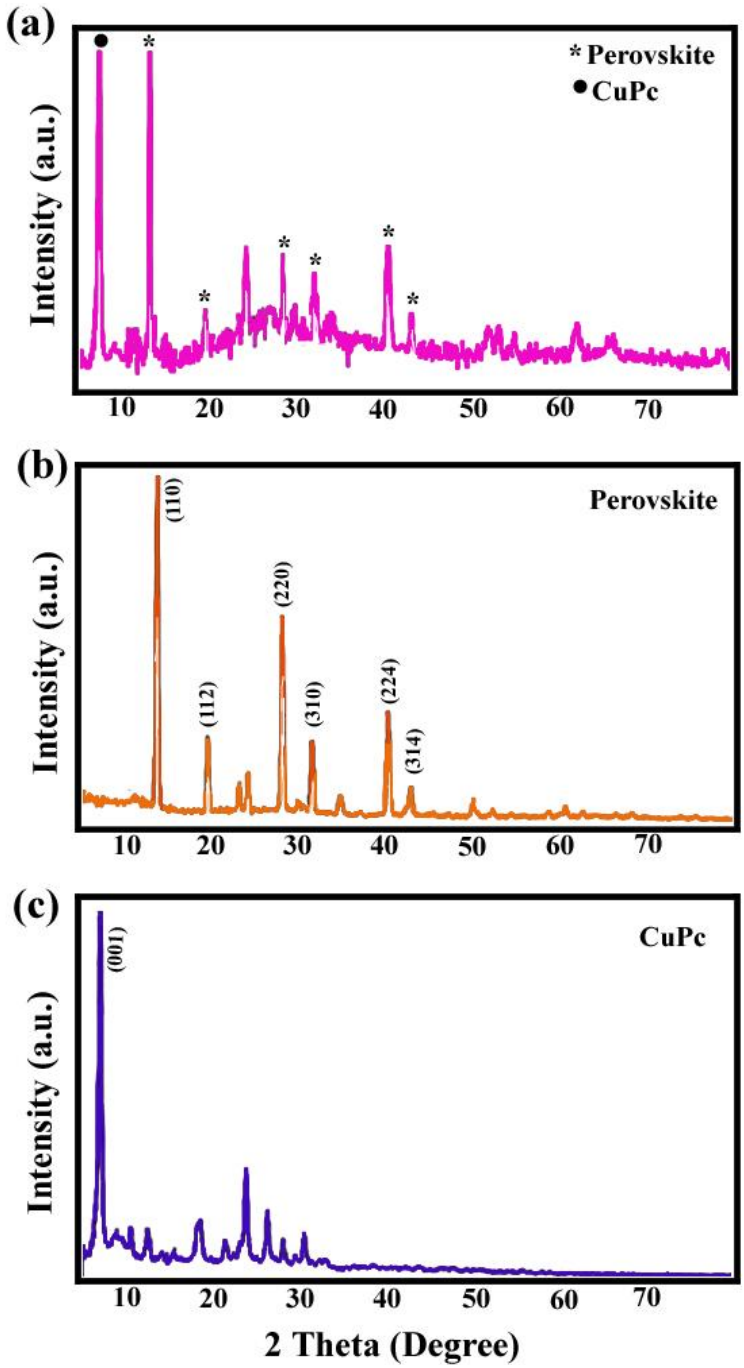

Fig. 5. (a-c) XRD patterns of ITO/Er:SnO_2/$CH_3NH_3PbI_3$/CuPc, ITO/Er:SnO_2/$CH_3NH_3PbI_3$, and CuPc.

metal dioxide film quality by minimizing surface-state traps, resulting in improved photo-generated electron collection [39, 40]. Fig. 6c shows the cross-sectional FESEM of Er-SnO_2 films. The electron transport layer with 160 nm thikness was deposited on ITO substrate, which improves electron release and ultimately contributes to the cell's increased efficiency and Fig. 6d indicates the EDS analysis of ITO/Er:SnO_2 layer that this layer was made up of Sn and Er elements.

Figs. 7a and d show the top-view FE-SEM images of the perovskite film and CuPc deposited on the untreated Er:SnO_2 ETL (<80nm). The perovskite film exhibits a uniform crystal size of ca. 400 nm along with a smooth coverage surface coverage. Also, the top FE-SEM of the perovskite layer demonstrates the presence of small crystals [41-43]. The XRD results suggest that this tiny crystal at the grain boundary is PbI_2. PbI_2 has the advantage of reducing the grain boundary, suppressing the hole (H^+) and electron (e^-) recombination at the interface, and consequently improves the Jsc of the device. According to a morphological comparison, there are no obvious changes in the crystal size of $MAPbI_3$ nor in the growth of the SnO_2 and Er:SnO_2-based ETLs. The crystal size of $MAPbI_3$ doesn't change in the SnO_2 and Er:SnO_2-based ETLs.

Fig. 7c displays a cross-sectional FE-SEM image of the ITO/Er:SnO_2/$MAPbI_3$/CuPc/Au device. The perovskite crystal's proximity to the compact

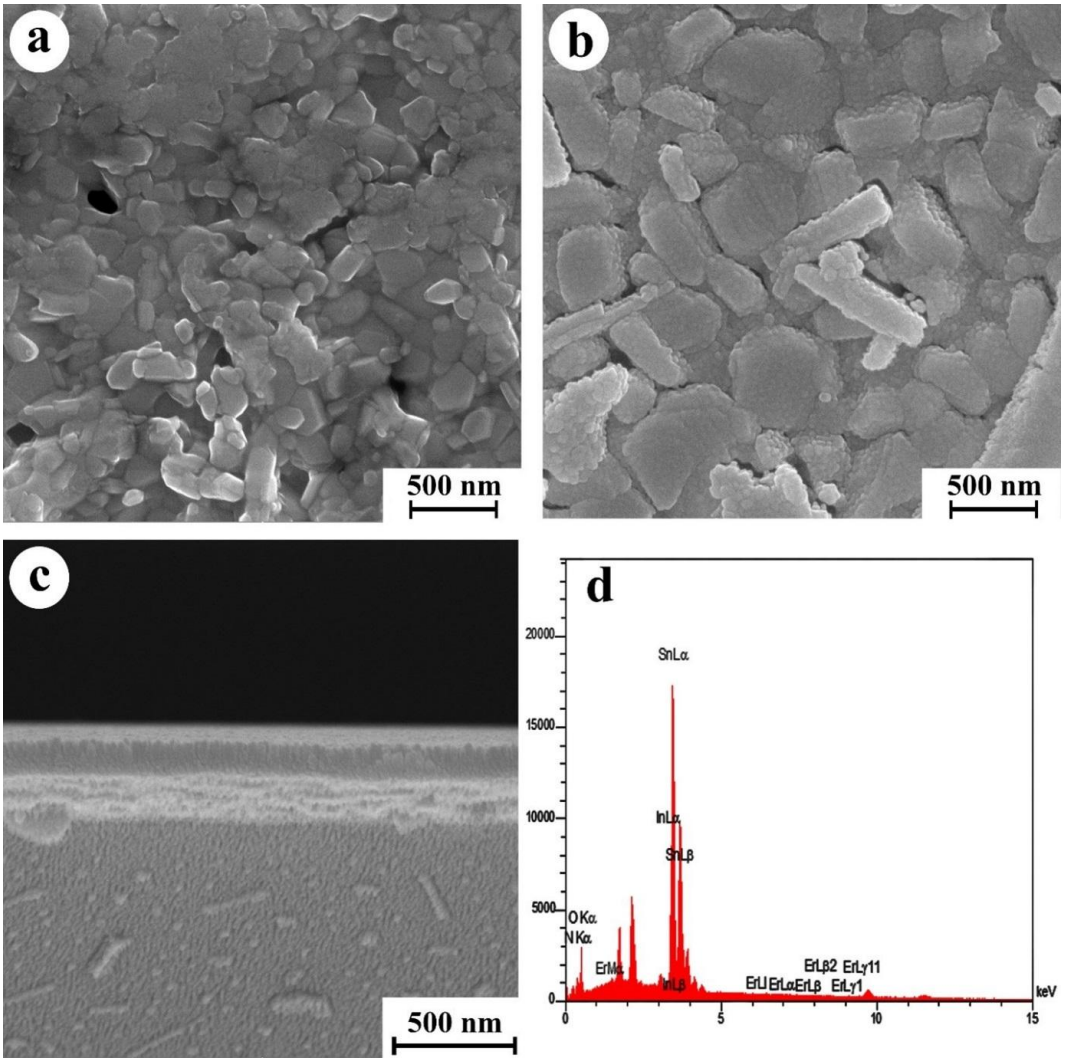

Fig. 6. (a and b) Top-view SEM images of SnO_2 and Er:SnO_2, and (c and d) SEM cross-sectional image and EDS analysis of Er:SnO_2 film.

Er:SnO_2 layer allows for better longitudinal carrier transport.

Fig. 7d shows the EDS analysis of ITO/Er:SnO_2/$MAPbI_3$/CuPc/Au layer shows that this layer was made up of Sn, Er, Cu, Iand Pb elements. The purity of as-synthesized ITO/SnO_2/$MAPBI_3$/CuPc/Au layer was confirmed by EDS result.

Fig. 8 presents the optical transmission spectra of SnO_2 from the wavelength of 300 nm to 800 nm. Erbium doping indicates an increase in transparency, which suggests that the Er^{+3} is beneficial for the optical transmittance

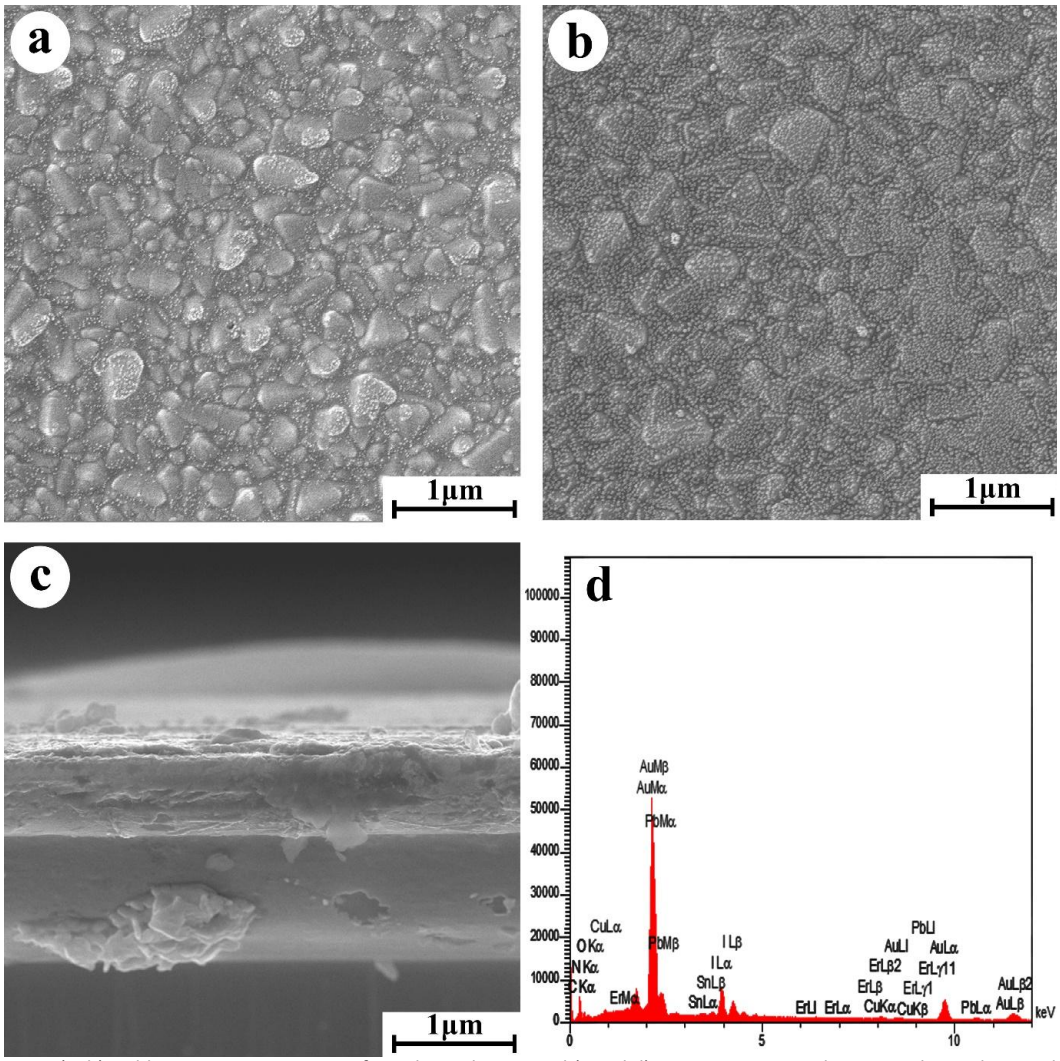

Fig. 7. (a, b) Field emission SEM images of $MAPbI_3$ and CuPc, and (c and d) SEM cross-sectional image and EDS elemental analysis of ITO/Er:SnO_2/$MAPbI_3$/CuPc/Au.

Table 1. Information on Mott-Schottky analysis of SnO_2 and 7.00% Er:SnO_2 thin films was measured using a 0.5 M KCl solution.

Sample	Band gap(eV)	Synthesis method	References
SnO_2:Er	3.8	Hydrothermal	[48]
$Sn_{1-x}Er_xO_2$ nanoparticles	3.73-3.91	Solgel	[49]
$Sn_{1-x}Er_xO_2$ thin films	3.99-4.02	Spray pyrolysis	[50]

performance of SnO_2. Er:SnO_2 samples with a high transparency enhance the electron transport. Doping SnO_2 with Er^{3+} has increased its energy band gap (3.6 eV), and it seems to enhance the protection of perovskite against harmful UV radiation in solar cells. Table 1 shows the characterization comparison of band gap of SnO_2 and E:SnO_2 with other similar work.

Electrochemical properties

In order to achieve the energy level of the new ETL which was applied, cyclic voltammogram (CV) of ETLs was measured. The CV reactions of the electrodes were investigated in several different conditions in 5.0 mmol L^{-1} Fe $(CN)_6^{3-/4-}$ (K_3Fe $(CN)_6$) redox electrode in 0.1 mol L^{-1} KCl solution (with pH of 6) at a scan rate of 50 mV s^{-1} between -0.4 and

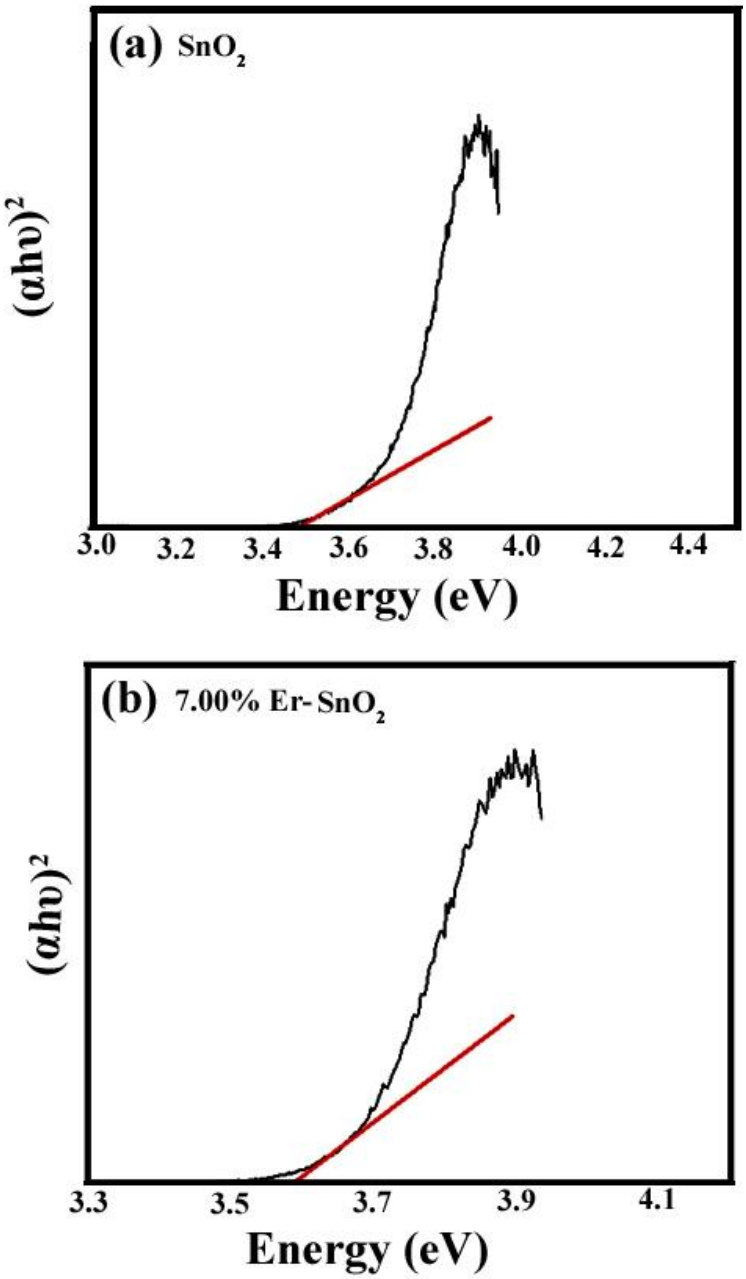

Fig. 8. The UV-visible absorption spectrum and tauc plot for a) SnO_2 and b) 7.00% Er:SnO_2 ETL.

+0.6. Cyclic voltammetry (CV) helps identifying improvements to the ETL surface. Well-defined CV cycles indicate a higher quality and defect-free surface which can potentially lead to increased device efficiency.

According to the CV, doping SnO_2 with erbium can improve the quality of thin layers by reduced oxidation and reduction peak magnitudes. This issue aligned with our prediction regarding the impact of lanthanide doping in electron transfer layers, as previously reported [44]. The cyclic voltammograms (CVs) of electron transporting layers (ETLs) incorporating different percentages of erbium are presented in Fig. 9a.

Following (CV) analysis, Mott-Schottky measurements were performed on electrodes exhibiting the optimal surface properties for each impurity concentration. This approach is crucial because Mott-Schottky analysis reveals key characteristics like carrier concentration, flat-band potential, energy levels, and conductivity type - all vital factors for selecting suitable semiconductors in electronic devices. The Mott-Schottky (M-S) technique allows us to determine essential semiconductor properties. The M-S analysis involves plotting the inverse square of the space-charge capacitance (Csc) as a function of the applied bias potential.

The slope of the Mott-Schottky (M-S) plot is a well-established approach for determining the semiconductor doping consistency N_D. Additionally, extrapolation of the linear region's intercept to the potential axis allows for the estimation of the flat-band potential (V_{fb}) based on the M-S relationship:

$$\frac{1}{c_{sc}^2} = \frac{2}{\varepsilon_0 \varepsilon r N_D}\left(V\text{-}V_{fb}\text{-}\frac{kT}{e}\right)$$

The equation uses various symbols to represent key properties of the semiconductor, including the number of charge carriers (N_D), a fundamental constant related to electron charge (e), the permittivity of empty space (ε_o), a material property affecting electrical fields (ε_r), and two potential values: the flat-band potential (V_{fb}) and the applied potential (V). Additionally, T shows the temperature of the operation (300 K), K refers to the Boltzmann's constant (1.38 × 10-23 J/K), and C_{SC} is the space charge capacity. In this

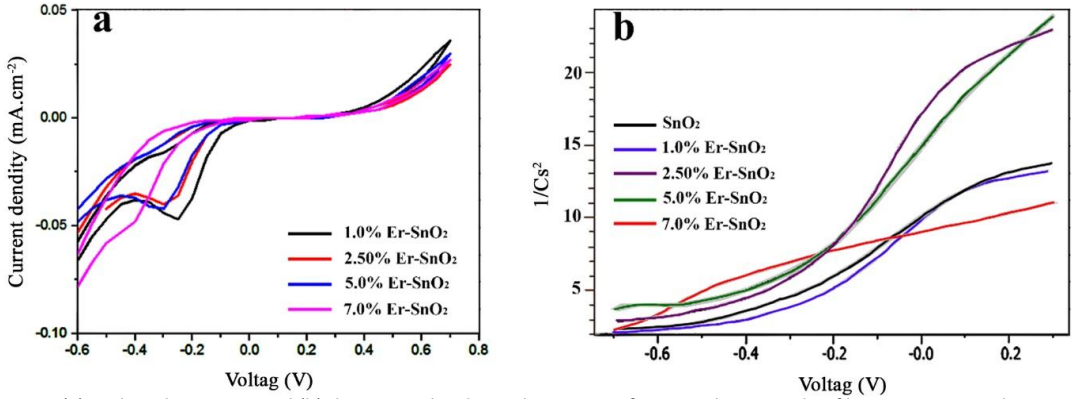

Fig. 9. (a) Cyclic voltammetry and (b) the Mott-Schottky analysis curve of SnO_2 and Er:SnO_2 thin films was measured using a 5.0 mmol L^{-1} $Fe(CN)_6^{-3/-4}$/K3Fe(CN)$_6$ redox electrode in a 0.1 mol L^{-1} KCl and 0.5 M KCl solution.

Table 2. Performance parameters of perovskite solar cells.

ETL	N_D(cm^{-3})	V_{fb}(V)	Intercept(V)
SnO_2	3.04E+17	-0.621	-0.653
1.00%Er:SnO_2	3.73E+17	-0.636	-0.662
2.5% Er:SnO_2	3.85E+17	-0.665	-0.69
5.00% Er:SnO_2	5.25E+17	-0.698	-0.723
7.00% Er:SnO_2	5.89E+17	-0.763	-0.789

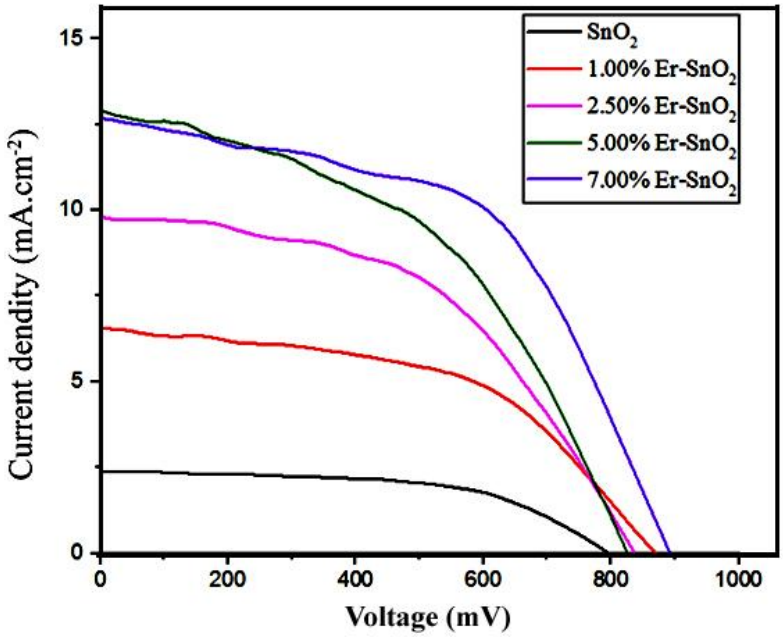

Fig. 10. J–V curves of ITO/Er:SnO_2/$MAPbI_3$/CuPc/Au solar cells.

Table 3. Characterization comparison of band gap of SnO_2 and E:SnO_2 with other similar work.

Device	Voc(mV)	Jsc(mA)	FF(%)	PCE(%)
SnO_2	755	2.40	55	1.05
1.00%Er:SnO_2	875	6.55	51	2.92
2.5% Er:SnO_2	845	9.81	49	4.04
5.00% Er:SnO_2	825	12.93	45	4.86
7.00% Er:SnO_2	895	12.68	53	6.05

study, the dielectric constant for SnO_2 film is 8.5 [30, 45]. The positive slopes of the curves suggest that all the films have an n-type conductivity. To gain a deeper understanding of carrier transport mechanisms in the potassium halide-doped SnO_2 thin films, we also determined the carrier density (N_D). Although the as-prepared layers are identical regarding the crystallinity, the carrier density for the 7.00% Er layer is higher and the defect density is expected to be lower. The increased V_{bi} suggests stronger charge separation and reduced carrier recombination, aligning well with the higher Voc [46]. Fig. 9b presents the graphs of Mott-Schottky analysis and the data extracted from this analysis is summarized in Table 2.

Fig. 10 and Table 3 provide the data on the photovoltaic performances of the Er:SnO_2-based PSCs. The PCE significantly increased from 1.05% (for pure SnO_2) to 6.05% when the SnO_2 was doped with Er (concentration of 7.00%). The pure SnO_2 ETL achieves a PCE of 1.05% with Jsc of 2.40 mA·cm^{-2}, V_{OC} of 795 mV, and FF of 55% when scanned in the reverse direction. By adding Er into the SnO_2 ETL, the PCE rapidly increased to 6.07% with the Jsc of 12.68 mA·cm^{-2}, V_{OC} of 895 mV, and FF of 53%. The higher electron conductivity and reduced resistance of the Er:SnO_2 ETL results in the improved J_{SC} and FF. The rise in V_{OC} is due to the upshifted conduction band level of Er:SnO_2 that is precisely aligned to the perovskite layer [47].

CONCLUSION

In this study Er was doped into the SnO_2 compact layer. Regulation of the Er^{+3} content in the $SnCl_4$ precursor solution contributes to the preparation and consequent application of Er:SnO_2 compact layers with varying doping concentrations to PSCs. SEM and XRD analyses were used to characterize

and analyze the surface morphology, chemical bonding, element composition, crystal structure, and crystallinity of SnO_2 compact layers. The J-V curves of PSCs based on the SnO_2 compact layer containing varying Er doping concentrations were subjected to testing and characterization. At a doping concentration of 7.00% Er, the Er-doped SnO_2 compact layer device demonstrated superior performance compared to devices that did not incorporate a doped SnO_2 layer. Therefore, this method can be used to various fields, such as solar energy conversion technologies, photo-electrochemical devices for water purification, and others.

ACKNOWLEDGEMENT

Authors are grateful to University of Kashan for financially supporting this work by Grant No. (463561-40).

CONFLICT OF INTERESTS

The authors declare that there is no conflict of interests regarding the publication of this manuscript.

REFERENCES

1. Jeon NJ, Noh JH, Kim YC, Yang WS, Ryu S, Seok SI. Solvent engineering for high-performance inorganic–organic hybrid perovskite solar cells. Nature Materials. 2014;13(9):897-903.
2. Saliba M, Matsui T, Seo J-Y, Domanski K, Correa-Baena J-P, Nazeeruddin MK, et al. Cesium-containing triple cation perovskite solar cells: improved stability, reproducibility and high efficiency. Energy and Environmental Science. 2016;9(6):1989-1997.
3. Gonzalez-Pedro V, Juarez-Perez EJ, Arsyad W-S, Barea EM, Fabregat-Santiago F, Mora-Sero I, et al. General Working Principles of CH_3/NH_3PbX_3 Perovskite Solar Cells. Nano Lett. 2014;14(2):888-893.
4. Jiang Q, Zhang X, You J. SnO_2: A Wonderful Electron Transport Layer for Perovskite Solar Cells. Small. 2018;14(31).
5. Zhang X, Wu T, Xu X, Zhang L, Tang J, He X, et al. Ligand-exchange TiO_2 nanocrystals induced formation of high-quality electron transporting layers at low temperature for efficient planar perovskite solar cells. Sol Energy Mater Sol Cells. 2018;178:65-73.
6. Dong Q, Shi Y, Wang K, Li Y, Wang S, Zhang H, et al. Insight into Perovskite Solar Cells Based on SnO_2 Compact Electron-Selective Layer. The Journal of Physical Chemistry C. 2015;119(19):10212-10217.
7. Calabrò E, Matteocci F, Palma AL, Vesce L, Taheri B, Carlini L, et al. Low temperature, solution-processed perovskite solar cells and modules with an aperture area efficiency of 11%. Sol Energy Mater Sol Cells. 2018;185:136-144.
8. Jiang Q, Zhang L, Wang H, Yang X, Meng J, Liu H, et al. Enhanced electron extraction using SnO_2 for high-efficiency planar-structure $HC(NH_2)_2PbI_3$-based perovskite solar cells. Nature Energy. 2016;2(1).
9. Yang G, Chen C, Yao F, Chen Z, Zhang Q, Zheng X, et al. Effective Carrier-Concentration Tuning of SnO_2 Quantum Dot Electron-Selective Layers for High-Performance Planar Perovskite Solar Cells. Adv Mater. 2018;30(14).
10. Ke W, Fang G, Liu Q, Xiong L, Qin P, Tao H, et al. Low-Temperature Solution-Processed Tin Oxide as an Alternative Electron Transporting Layer for Efficient Perovskite Solar Cells. Journal of the American Chemical Society. 2015;137(21):6730-6733.
11. Wang Y, Duan C, Li J, Han W, Zhao M, Yao L, et al. Performance Enhancement of Inverted Perovskite Solar Cells Based on Smooth and Compact $PC_{61}BM$:SnO_2 Electron Transport Layers. ACS Applied Materials and Interfaces. 2018;10(23):20128-20135.
12. Liu Z, Sun B, Liu X, Han J, Ye H, Tu Y, et al. 15% efficient carbon based planar-heterojunction perovskite solar cells using a TiO_2/SnO_2 bilayer as the electron transport layer. Journal of Materials Chemistry A. 2018;6(17):7409-7419.
13. ZnO/SnO_2 Double Electron Transport Layer Guides Improved Open Circuit Voltage for Highly Efficient $CH_3NH_3PbI_3$-Based Planar Perovskite Solar Cells. American Chemical Society (ACS).
14. Dagar J, Castro-Hermosa S, Gasbarri M, Palma AL, Cina L, Matteocci F, et al. Efficient fully laser-patterned flexible perovskite modules and solar cells based on low-temperature solution-processed SnO_2/mesoporous-TiO_2 electron transport layers. Nano Research. 2018;11(5):2669-2681.
15. Tavakoli MM, Giordano F, Zakeeruddin SM, Grätzel M. Mesoscopic Oxide Double Layer as Electron Specific Contact for Highly Efficient and UV Stable Perovskite Photovoltaics. Nano Lett. 2018;18(4):2428-2434.
16. Song S, Kang G, Pyeon L, Lim C, Lee G-Y, Park T, et al. Systematically Optimized Bilayered Electron Transport Layer for Highly Efficient Planar Perovskite Solar Cells (η = 21.1%). ACS Energy Letters. 2017;2(12):2667-2673.
17. Xie J, Huang K, Yu X, Yang Z, Xiao K, Qiang Y, et al. Enhanced Electronic Properties of SnO_2 via Electron Transfer from Graphene Quantum Dots for Efficient Perovskite Solar Cells. ACS Nano. 2017;11(9):9176-9182.
18. Zhao X, Tao L, Li H, Huang W, Sun P, Liu J, et al. Efficient Planar Perovskite Solar Cells with Improved Fill Factor via Interface Engineering with Graphene. Nano Lett. 2018;18(4):2442-2449.
19. Wang Y, Zhang X, Jiang Q, Liu H, Wang D, Meng J, et al. Interface Engineering of High-Performance Perovskite Photodetectors Based on PVP/SnO_2 Electron Transport Layer. ACS Applied Materials and Interfaces. 2018;10(7):6505-6512.
20. Huang C, Lin P, Fu N, Sun K, Ye M, Liu C, et al. Ionic liquid modified SnO_2 nanocrystals as a robust electron transporting layer for efficient planar perovskite solar cells. Journal of Materials Chemistry A. 2018;6(44):22086-22095.
21. Zeng X, Zhou T, Leng C, Zang Z, Wang M, Hu W, et al. Performance improvement of perovskite solar cells by employing a CdSe quantum dot/PCBM composite as an electron transport layer. Journal of Materials Chemistry A. 2017;5(33):17499-17505.
22. Lee Y, Paek S, Cho KT, Oveisi E, Gao P, Lee S, et al. Enhanced charge collection with passivation of the tin oxide layer in planar perovskite solar cells. Journal of Materials Chemistry A. 2017;5(25):12729-12734.
23. Wang P, Zhao J, Liu J, Wei L, Liu Z, Guan L, et al. Stabilization of organometal halide perovskite films by SnO_2 coating with inactive surface hydroxyl groups on ZnO nanorods. J Power Sources. 2017;339:51-60.

24. Park M, Kim J-Y, Son HJ, Lee C-H, Jang SS, Ko MJ. Low-temperature solution-processed Li-doped SnO_2 as an effective electron transporting layer for high-performance flexible and wearable perovskite solar cells. Nano Energy. 2016;26:208-215.
25. Chen H, Liu D, Wang Y, Wang C, Zhang T, Zhang P, et al. Enhanced Performance of Planar Perovskite Solar Cells Using Low-Temperature Solution-Processed Al-Doped SnO_2 as Electron Transport Layers. Nanoscale Research Letters. 2017;12(1).
26. Xiong L, Qin M, Chen C, Wen J, Yang G, Guo Y, et al. Fully High-Temperature-Processed SnO_2 as Blocking Layer and Scaffold for Efficient, Stable, and Hysteresis-Free Mesoporous Perovskite Solar Cells. Adv Funct Mater. 2018;28(10).
27. Liu X, Zhang Y, Shi L, Liu Z, Huang J, Yun JS, et al. Exploring Inorganic Binary Alkaline Halide to Passivate Defects in Low-Temperature-Processed Planar-Structure Hybrid Perovskite Solar Cells. Advanced Energy Materials. 2018;8(20).
28. Halvani Anaraki E, Kermanpur A, Mayer MT, Steier L, Ahmed T, Turren-Cruz S-H, et al. Low-Temperature Nb-Doped SnO_2 Electron-Selective Contact Yields over 20% Efficiency in Planar Perovskite Solar Cells. ACS Energy Letters. 2018;3(4):773-778.
29. Wang P, Wang J, Zhang X, Wang H, Cui X, Yuan S, et al. Boosting the performance of perovskite solar cells through a novel active passivation method. Journal of Materials Chemistry A. 2018;6(32):15853-15858.
30. Guo Z, Gao L, Zhang C, Xu Z, Ma T. Low-temperature processed non-TiO_2 electron selective layers for perovskite solar cells. Journal of Materials Chemistry A. 2018;6(11):4572-4589.
31. Shin SS, Yeom EJ, Yang WS, Hur S, Kim MG, Im J, et al. Colloidally prepared La-doped $BaSnO_3$ electrodes for efficient, photostable perovskite solar cells. Science. 2017;356(6334):167-171.
32. Gao X-X, Ge Q-Q, Xue D-J, Ding J, Ma J-Y, Chen Y-X, et al. Tuning the Fermi-level of TiO_2 mesoporous layer by lanthanum doping towards efficient perovskite solar cells. Nanoscale. 2016;8(38):16881-16885.
33. Sun H, Deng K, Zhu Y, Liao M, Xiong J, Li Y, et al. A Novel Conductive Mesoporous Layer with a Dynamic Two-Step Deposition Strategy Boosts Efficiency of Perovskite Solar Cells to 20%. Adv Mater. 2018;30(28).
34. Guo X, Du J, Lin Z, Su J, Feng L, Zhang J, et al. Enhanced efficiency and stability of planar perovskite solar cells using SnO_2:$InCl_3$ electron transport layer through synergetic doping and passivation approaches. Chem Eng J. 2021;407:127997.
35. Mahmood M, Islam MT, Sadek MS, Noor K, Baharuddin MHB, Ibrahim M, et al. Advancing perovskite solar cells: Unveiling the superior efficiency of copper-doped Strontium Titanate as a novel ETL. Solar Energy. 2024;279:112806.
36. Arshad Z, Shakir S, Khoja AH, Javed AH, Anwar M, Rehman A, et al. Performance Analysis of Calcium-Doped Titania (TiO_2) as an Effective Electron Transport Layer (ETL) for Perovskite Solar Cells. Energies. 2022;15(4):1408.
37. Esmaeili-Zare M, Amiri O. Rare earth–based compounds for solar cells. Advanced Rare Earth-Based Ceramic Nanomaterials: Elsevier; 2022. p. 365-393.
38. Mahdipour M, Esmaeili-Zare M, Hamadanian M. Modification of Solar Energy and Photoelectrochemical Water Splitting Properties: Using Fto/Er-TiO_2/$MAPbI_3$/Cupc/Au as Modified Photoelectrode. Elsevier BV; 2024.
39. Yuqi S, Mamat M, Baikeli Y, Xiaerding F. Effects of doping of Sm, Y, Ce and La on crystal structure, phase and photocatalytic performance of TiO_2 powders prepared by sol-gel method. Phys Lett A. 2024;525:129929.
40. Zhao L, Li G, Li F, Yao M. Enhanced visible light photoactivity of TiO_2/SnO_2 films by tridoping with Y/F/Ag ions. Journal of Rare Earths. 2022;40(4):616-625.
41. Zhang K, Zhao Y, Duan R, Huang P, Zhu K, Li Z, et al. Improve the crystallinity and morphology of perovskite films by suppressing the formation of intermediate phase of $CH_3NH_3PbCl_3$. Org Electron. 2019;68:96-102.
42. Ren X, Yang Z, Yang D, Zhang X, Cui D, Liu Y, et al. Modulating crystal grain size and optoelectronic properties of perovskite films for solar cells by reaction temperature. Nanoscale. 2016;8(6):3816-3822.
43. Zou Y, Yuan S, Buyruk A, Eichhorn J, Yin S, Reus MA, et al. The Influence of CsBr on Crystal Orientation and Optoelectronic Properties of $MAPbI_3$-Based Solar Cells. ACS Applied Materials and Interfaces. 2022;14(2):2958-2967.
44. Bibi Jaffri S, Shahzad Ahmad K, Abrahams I, Tighezza AM. [Gd^{3+}–Ho^{3+}-Dy^{3+}]:$CsPbI_{2.2}Br_{0.8}$: Lanthanide impelled stabilization of perovskite material for sustainable energy harvesting, generation, and charge storage. Sustainable Energy Technologies and Assessments. 2023;60:103566.
45. Bai C, Dong W, Cai H, Zu C, Yue W, Li H, et al. Electrochemical Reduction and Ion Injection of Annealing-Free SnO_2 for High Performance Perovskite Solar Cells. Advanced Energy Materials. 2023;13(26).
46. Xu Y, Rui Y, Wang X, Li B, Jin Z, Wang Y, et al. Dual passivation of SnO_2/Perovskite heterogeneous interfacial defects for efficient perovskite solar cells. Sol Energy Mater Sol Cells. 2023;250:112088.
47. Shah SAA, Sayyad MH, Sun J, Guo Z. Recent advances and emerging trends of rare-earth-ion doped spectral conversion nanomaterials in perovskite solar cells. Journal of Rare Earths. 2022;40(11):1651-1667.
48. Tuan PV, Hieu LT, Nga LQ, Dung ND, Ha NN, Khiem TN. Hydrothermal synthesis and characteristic photoluminescence of Er-doped SnO_2 nanoparticles. Physica B: Condensed Matter. 2016;501:34-37.
49. Sambasivam S, Kim SB, Jeong JH, Choi BC, Lim KT, Kim SS, et al. Effect of Er^{3+} doping in SnO_2 semiconductor nanoparticles synthesized by solgel technique. Current Applied Physics. 2010;10(6):1383-1386.
50. Sambasivam S, Maram PS, Muralee Gopi CVV, Obaidat IM. Effect of erbium on the structural, morphological, and optical properties of SnO_2 thin films deposited by spray pyrolysis. Optik. 2020;202:163596.